How can the thermal mixing of two sprays be characterized? Application of combined three-color LIF thermometry and phase Doppler Analyzer

Alexandre Labergue, Alain Delconte, Fabrice Lemoine

How can the thermal mixing of two sprays be characterized? Application of combined three-color LIF thermometry and phase Doppler Analyzer.

Alexandre Labergue[1,2*], Alain Delconte[1,2], Fabrice Lemoine[1,2]

1: Université de Lorraine, LEMTA, UMR 7563, Vandoeuvre-Lès-Nancy, F-54504, France

2: CNRS, LEMTA, UMR 7563, Vandoeuvre-Lès-Nancy, F-54504, France

* Corresponding author: alexandre.labergue@univ-lorraine.fr

Abstract The aim of this experimental work was to demonstrate the ability of three-color LIF (3cLIF) thermometry to study the thermal mixing of two non-isothermal water sprays. Combined 3cLIF-PDA measurements were also implemented to derive correlations between droplet size and temperature. Both sprays had different characteristics in terms of flow rate and droplet size distribution. The liquid spray was successively pre-heated and the other spray was maintained and injected at ambient temperature. The thermal mixing will be discussed in the light of a wide set of experimental results obtained under various experimental conditions, including different liquid flow rates, droplet size distributions and droplet concentrations. To analyze the potential effect of droplet coalescence on the mean local liquid temperature, both sprays were alternatively seeded with fluorescent dye. In the present case, direct heat transfer between both sprays due to droplet coalescences was found to remain marginal but indirect heat transfer was highlighted.

1. Introduction

In the current context, the characterization of heat and mass transfer that occurs in polydisperse sprays is an important challenge for use in an increasing number of engineering applications like internal combustion engines [1-3], the cooling of hot surfaces for dissipation of high heat fluxes [4; 5] or in several spray processes like drying and mixing highly reactive reagents when droplets are used as micro-chemical reactors. In the latter application, chemical reactions may be involved and so, heat transfer is a critical issue that needs to be characterized appropriately using dedicated experiments. In addition, the spray local temperature, droplet size distribution and liquid mass flux or droplet concentration all need to be measured. Phase Doppler instruments have progressed over the last few decades in characterizing droplet size, mass flux or concentration but scalar measurements like droplet temperature or chemical composition are still in development and remain difficult to implement. Indeed, few techniques are currently able to properly measure droplet temperature. With sprays, Global Rainbow Thermometry (GRT) can be used to quantify the refractive index using the angular position of the rainbow provoked by the scattered light of droplets crossing an extended probe volume and hence the relation between temperature and refractive index enables the calculation of the local spray temperature averaged over the extended probe volume [7; 8]. Another method is to use temperature-sensitive fluorescent dyes, seeded in the liquid and excited by a laser tuned on the absorption spectrum. Measuring intensities on droplets appears not to be relevant since the fluorescence is roughly proportional to the liquid volume in the line of sight of the collecting optics. Ratiometric methods have also been extensively developed and some of these techniques are based on exciplex [11; 12] or alternatively two fluorescent tracers [13; 14]. The present paper considers the combination of two-color laser-induced fluorescence (2cLIF) thermometry [3] and Phase Doppler Analyzer (PDA) in order to obtain the droplet temperature per size class. The 2cLIF uses a single temperature sensitive fluorescent dye and the fluorescence emission is collected on two spectral bands in order to derive a ratio that depends only in principle on the liquid temperature. The technique was successfully applied in the case of single evaporating or combusting droplets [15; 16]. However, it was demonstrated that the direct application of the

2cLIF in the case of polydisperse sprays was not a straightforward procedure [17; 18]. Firstly, a significant residual dependence of the fluorescence ratio on the droplet size was highlighted, especially for droplets diameter lower than 100 µm [17] and secondly, it was also demonstrated that if the depth of field of the fluorescence collecting optics was too large this was likely to induce a significant bias on the measurements [18]. A particular optical set-up was developed which allows the significant reduction of bias:

- the signal collected on a third spectral band of detection (the technique being called 3cLIF) is used to empirically correct the residual diameter dependence.
- the use of a long-distance microscope as a fluorescence collecting optics, with a lower depth of field, significantly reduces the bias of the technique.

In the present work, combined 3cLIF and PDA will be applied to investigate the particular configuration where two non iso-thermal water sprays are mixed together. A first spray is injected at ambient temperature simultaneously with another overheated spray. Both sprays had different characteristics in terms of flow rate, droplet size distributions and droplet concentration. More precisely, the aim of the experiments was to study how heat transfer between two sprays mixed together can be investigated. The influence of the flow rate and droplet size distribution was also a subject of study.

2. Principles of the LIF thermometry

2.1 Two-color LIF thermometry

The mean features of the 2cLIF thermometry are summarized in this section. Further details are available in previous publications [15; 16]. The liquid is preliminary seeded by a temperature sensitive fluorescent dye at a low concentration. In the present work, the liquid is deionised water seeded with sulforhodamine B at a concentration of 5.10^{-6} mo.L^{-1}. The fluorescence is induced by the green line of an argon ion laser (λ = 514.5 nm). The fluorescence spectrum of sulforhodamine B is broadband and presents a temperature-dependent shape. Thus, the fluorescence intensity I_{fi} collected on a spectral band [λ_{i1}; λ_{i2}] can be expressed by [15]:

$$I_{fi}(T) = K_{opt,i} K_{spec,i} V_c I_o C f_i(T) \quad (1)$$

where I_0 is the local laser excitation intensity, C the fluorescent dye concentration, T the absolute temperature and V_c the collection volume of the fluorescence photons. This later is defined as the intersection of the illuminated part of the droplet volume in the field of view of the fluorescence collection optics. $K_{opt,i}$ and $K_{spec,i}$ are parameters influenced respectively by the optical layout and the fluorescence properties of the fluorescent tracers. The function $f_i(T)$ describes the temperature dependence of the fluorescence on the spectral band i that can be empirically approximated by [16]:

$$f_i(T) \approx e^{\frac{a_i}{T^2}+\frac{b_i}{T}}, \quad (2)$$

where a_i and b_i are two coefficients that characterize the temperature sensitivity of the fluorescence signal on the spectral band i. The parameters C, V_c and I_0 are not constant when a potentially evaporating droplet moves into the laser excitation volume and therefore remain unknown. These parameters can be removed by simultaneously collecting the fluorescence signal on two spectral bands, respectively I_{f1} and I_{f2} and by calculating their ratio R_{12}:

$$R_{12} = \frac{I_{f1}}{I_{f2}} = \frac{K_{opt,1} K_{spec,1} f_1(T)}{K_{opt,2} K_{spec,2} f_2(T)} = \frac{K_{opt,1} K_{spec,1}}{K_{opt,2} K_{spec,2}} e^{\frac{a_{12}}{T^2}+\frac{b_{12}}{T}} \quad (3)$$

where a_{12} and b_{12} respectively denote $(a_1 - a_2)$ and $(b_1 - b_2)$. In *eqn* (3), the ratio R_{12} depends solely on temperature. In the present study, the selected spectral bands are:

- Band 1: [535 nm; 545 nm]
- Band 2: [615 nm; 750 nm].

Using these bands gives a high level of sensitivity in the fluorescence ratio on temperature. A calibration, conducted in a similar process to the one described in [19], leads to a temperature

sensitivity of about 0.9%/K. Finally, a single reference R_{120} measurement at a known temperature T_0 was used to eliminate both constants $K_{opt,i}$ and $K_{spec,i}$ in *eqn* (3). The normalized ratio R_{12}/R_{120} is given by:

$$\frac{R_{12}}{R_{12o}} = \frac{f_{12}(T)}{f_{12}(T_0)} \quad (1)$$

2.2 Combined droplet size and depth of field bias

A recently study [17] highlighted a residual effect of the droplet diameter on the fluorescence ratio, not included in *eqn* (3). This effect is attributed to a significant distortion of the fluorescence spectrum and remains poorly explained [17]. The deviation from the previous model is larger when smaller droplets are studied namely those typically under D = 100 µm. *Fig. 1*, extracted from [17], shows the evolution of the normalized fluorescence ratio of single calibrated water droplets (seeded with sulforhodamine B) as a function of the diameter D [17]. A significant increase in the fluorescence ratio was observed when decreasing the droplet diameter; otherwise the normalized fluorescence ratio tended to 1 for the largest droplet diameters. To account for the effect of the droplet size on the fluorescence ratio, an empirical function $g_{12}(D)$ was added in *eqn*. (4) [17]:

$$\frac{R_{12}}{R_{12o}} = \frac{f_{12}(T)}{f_{12}(T0)} g_{12}(D) \quad (5)$$

The experimental determination of the function $g_{12}(D)$ will be described in a later section.

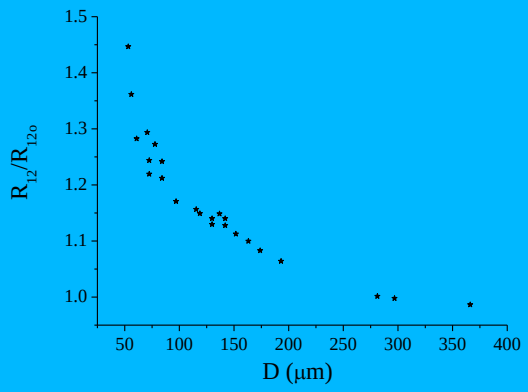

Figure 1: *Evolution of the normalized fluorescence ratio as a function of the droplet diameter of calibrated single droplets* [17].

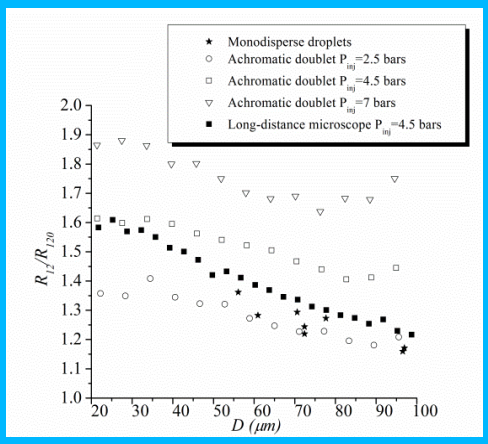

Figure 2: *Results of LIF/PDA measurements obtained with the use of an achromatic doublet and a long-distance microscope as collection optics: evolution of the fluorescence ratio as a function of the droplet diameter* [18].

Moreover, a study presented in [18] shows how a significant bias in the measurements of the fluorescence ratio R_{12} can be induced if the depth of field of the fluorescence collection optics is too large. This second phenomenon was investigated by using the combined LIF-PDA measurements previously developed and tested in [3]. *Fig. 2* depicts the evolution of the normalized fluorescence ratio R_{12}/R_{120} plotted as a function of the droplet diameter class measured in a spray for three injection pressures linked to an increase of the droplet concentration [18]. The shift towards higher ratio values which was observed when the pressure was increased can be attributed to an additional fluorescence contribution induced by Mie scattering of the incident laser light, coming from the off field of the collection optics. This contribution was found to increase with droplet concentration and depth of field dimension. Furthermore, the contribution of the off-field fluorescence, mainly linked to small droplets, tended to increase the fluorescence ratio value due to the bias related to the droplet size. The use of a long-distance microscope (QM-100; Questar®) with a much lower depth

of field enabled us to minimize the unwanted fluorescence contribution. *Fig. 2* shows an example of data obtained by means of a long-distance microscope with an injection pressure of 4.5 bars (symbols (■)).

2.3 Three-color LIF thermometry

A comprehensive survey of the 3cLIF technique is described in [18]. A function which takes into account the non-linear effect of the droplet size on the fluorescence ratio $g_{12}(D)$ was introduced. This unknown function was determined using an empirical approach. The basic idea was to use a third spectral band to determine a second normalized fluorescence ratio:

$$\frac{R_{32}}{R_{32o}} = \frac{f_{32}(T)}{f_{32}(T_o)} g_{32}(D) \quad (6)$$

The third spectral band was selected in order to minimize the temperature sensitivity of the ratio R_{32} represented by the function $f_{32}(T)$. For the selected band, *i.e.* [555 nm; 575nm], the temperature sensitivity was around 0.1 %/°C, which is lower than $f_{12}(T)$. Similarly, the reference R_{320} was taken in the same cell and at the same temperature T_0 as for R_{120}. Moreover, $g_{32}(D)$ was different from $g_{12}(D)$ and therefore the ratio R_{32} had a different sensitivity on the droplet size when compared to $g_{12}(D)$. As mentioned in [18], an empirical relationship between functions $g_{12}(D)$ and $g_{32}(D)$ can be determined experimentally by measuring the corresponding normalized fluorescence ratios for several droplet diameters under isothermal conditions. This produces monotonous evolution which can be easily interpolated by a second order polynomial:

$$g_{12} = \alpha {g_{32}}^2 + \beta g_{32} + \gamma \quad (7)$$

Finally, by combining *eqns* (5), (6) and (7) we determined a relation depending only on temperature:

$$\frac{R_{12}}{R_{12o}} \frac{f_{12}(T)}{f_{12}(T_o)} = \alpha \left[\frac{f_{32}(T_o)}{f_{32}(T)} \frac{R_{32}}{R_{32o}} \right]^2 + \beta \left[\frac{f_{32}(T_o)}{f_{32}(T)} \frac{R_{32}}{R_{32o}} \right] + \gamma \quad (8)$$

α, β and γ were empirically determined and *eqn* (8) can be solved to determine the temperature from the measurements of the ratios R_{12} and R_{32}.

3. Application for mixing of two non-isothermal sprays

3.1 Spray mixing facilities

Two different water sprays, in terms of flow rates, droplet size distributions and droplet concentration were used. Both sprays were full cone and generated by Danfoss® swirled nozzles commonly used for burners. The nozzles were supplied by independent pressurized tanks in order to control the flow rate of each spray. For the work presented here, the first spray, referred as spray (1), was operated with a flow rate Q_1 = 20 ml/min whereas, for the second spray, referred as spray (2), two flow rate values Q_2 were used (Q_2 = 40 ml/min and Q_2 = 60 ml/min). A heat exchanger was used to pre-heat the water of one spray whereas the liquid of the second spray was kept at ambient temperature. Both sprays were injected downwards at an angle of 10° from the vertical direction (*Fig. 3a*). The vertical *Z*-axis defines the median line of both nozzles centerlines (see gray dash lines in *Fig. 3a*). The origin of the *X-Y-Z* axis is defined at the intersection of the horizontal plan containing both nozzles exit with the median line, *i.e. Z*-axis. The intersection point of the inner edge of both sprays was located at *Z* = 20 mm. *Fig. 3b* depicts, in a top view, the optical receivers for LIF and PDA measurements.

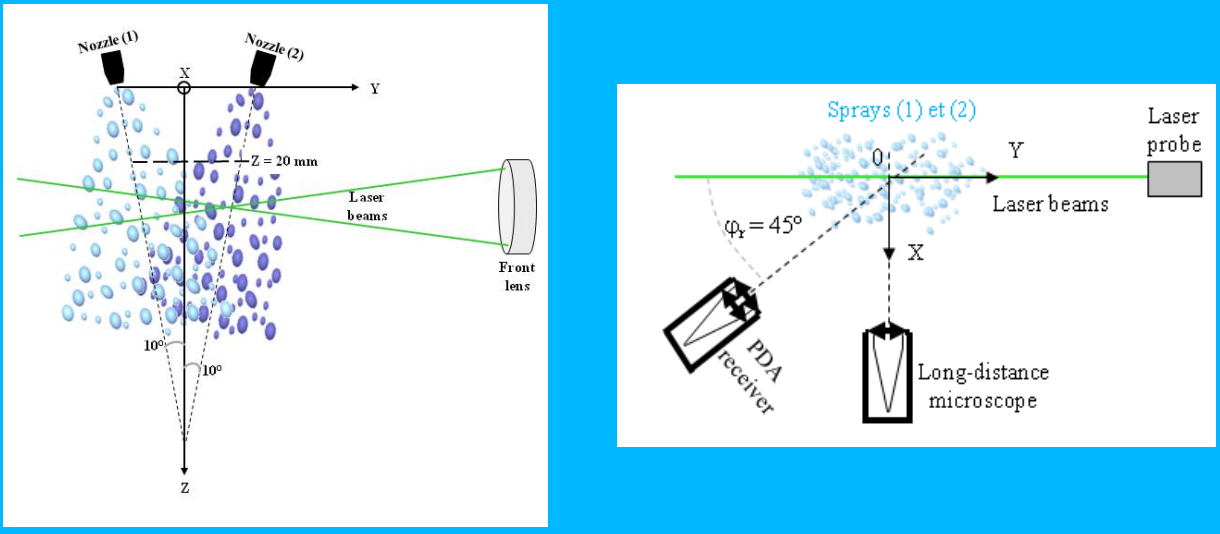

(a) (b)

Figure 3: *Spray mixing facilities (a) and top view of optical devices for 3cLIF and PDA detection (b).*

3.2 Geometry of the LIF and PDA detection volumes

For LIF and PDA measurements, an argon ion laser tuned at $\lambda = 514.5$ nm was used in order to obtain the common illuminated excitation volume. The latter was obtained by using a LDA transmitter probe (Dantec-dynamics Fiber-Flow® probe) with a frontal lens having a focal length f_e of 310 mm.

The vertical component of the droplet velocity (along the *Z*-axis) and the droplet diameter were both measured using a commercial Phase Doppler Analyser (PDA) manufactured by Dantec-Dynamics®. The system includes a classic reception optical device and a P80 signal processor. The receiver was positioned at a scattering angle $\varphi_r = 45°$ in order to operate in the first refraction mode. *Table 1* gives the characteristics of the PDA optical configurations. In this configuration, the PDA detection volume is defined by the intersection of the illuminated volume and the projection of a slit aperture (width $L_s = 120$ µm) located in the focal point of the receiving optics. If we take into account the magnification β_{PDA} and the angle of the receiver φ_r, the image of the slit (approximated as an obliquely truncated cylinder) along the excitation volume had a width $l_s = 274$ µm (*Fig. 4*).

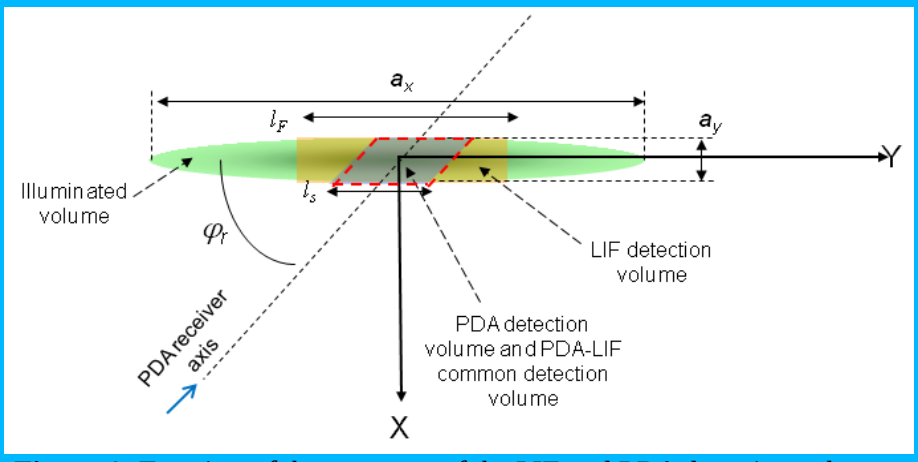

Figure 4: *Top view of the geometry of the LIF and PDA detection volumes.*

The fluorescence signal was collected at a right angle by using a long-distance microscope (QM-100; Questar®) at a working distance of 300 mm and coupled with an optical fiber having a core

diameter D_F = 70 µm (*Fig. 6*). In this case, the LIF detection volume is the intersection of the illuminated volume with the projected image of the optical fiber core (also approximated as a cylinder). At our working distance, the magnification β_{LIF} was 6.15 leading to a diameter of the fiber core image l_F = 430 µm (*Fig. 4*).
The common 3cLIF-PDA measurement volume is the superimposition of both LIF and PDA detection volumes. As a result, due to the very large LIF detection volume, the common detection volume is therefore the PDA detection volume (*Fig. 4*).

Emission focal length, f_e (mm)	*310*
Beam spacing, b_s (mm)	*60*
Reception focal length, f_r (mm)	*500*
Magnification, β_{PDA}	*1.60*
Scattering angle, φ_r (°)	*45*
Maximum detectable droplet diameter, D_{max} (mm)	*0.180*
Laser illuminated volume size based on 1/e² (mm)	
Size in *Z* and *Y* directions $a_z = a_x$	*0.152*
Size in *X* direction a_y	*1.562*

Table 1: *Characteristics and optical configuration of the PDA*

3.3 LIF data processing

The collected signal guided by the optical fibre was then high pass filtered (Chroma®, HQ 522 LP) in order to remove the light scattered at the laser wavelength. The remaining fluorescence signal was split into the three spectral bands mentioned in sections *2.2* and *2.3* by means of a set of dichroic and interference filters (*Fig. 6*). The fluorescence signal was detected by means of three photomultiplier tubes and digitalized with a frequency of 5 MHz for real time processing. A threshold was fixed significantly above the noise level of the channels of detection. If a sequence had more than ten consecutive samples above this threshold, it was considered to have come from droplets. The integration of samples, on each channel during the transit time T_t of a droplet within the detection volume, defines the fluorescence intensity I_f (*Fig. 5*). The fluorescence ratios R_{12} and R_{32} were then calculated as follows:

$$R_{ij} = \frac{I_{fi}}{I_{fj}} = \frac{\sum_{k=1}^{n} I_{fi,k-N_i}}{\sum_{k=1}^{n} I_{fj,k-N_j}} \qquad (9)$$

where $I_{fi,k}$ and $I_{fj,k}$ were respectively the fluorescence intensities integrated on the k^{th} droplet crossing the detection volume. n is the number of droplets detected during the acquisition period. N_i and N_j are the average dark noise values on the corresponding spectral bands. In [18], the uncertainty concerning the fluorescence ratio was evaluated as being around 1%. Typically, this would lead to an error of about ± 5°C for temperature.

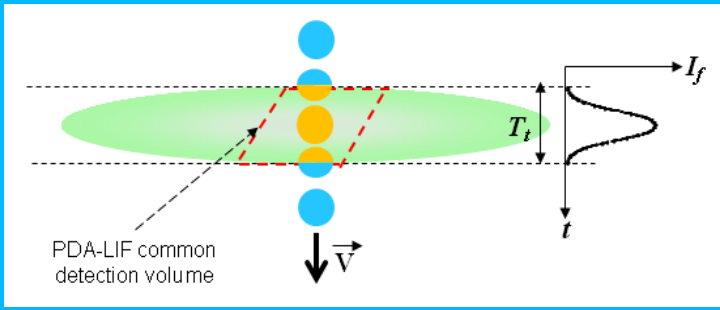

Figure 5: *Definition of the fluorescence intensity induced by the transit of a droplet crossing the detection volume.*

3.5 Combined LIF and PDA measurements

The optical arrangements and acquisition chain for combined LIF and PDA measurements are presented in *Fig*. 6. A full description of the principle and implementation can be found in [3]. The combined 3cLIF-PDA system provides two data files recorded with the same time base. One corresponds to the droplet velocity and diameters measured by the PDA and the other to the fluorescence intensities integrated into the droplet transit time within in the common detection volume for the three spectral bands of detection. Droplets detected simultaneously by PDA and 3cLIF were identified on the basis of their arrival time and their transit time. Then, a fixed number of droplet size classes were defined and the fluorescence intensity was averaged on each channel following *eqn*. (9). This meant that an average fluorescence ratio could be associated to a given droplet size class. An important point to note regarding technique is the common droplet size range that can be detected by both techniques. Indeed, when a droplet crosses the common LIF and PDA detection volume, the signal collected by the PDA and LIF is roughly proportional to D^2 and D^3 respectively. Based on ray tracing calculation, it was demonstrated that the fluorescence signal is proportional to $D^{2.8}$ [18]. Thus, the wider dynamic range of the LIF was found to limit the combined measurements in terms of droplets sizes. Consequently, only a limited range of the droplet size distribution can be simultaneously detected by LIF and PDA. [18] proposes a method for determining and optimizing dynamic detection. Here, the maximum detectable droplet diameter D_{max} was about 110 µm and the minimum droplet diameter D_{min} was roughly 20 µm (*Fig. 7*). Typically, a reliable acquisition sequence corresponds to about 50 000 common droplets. This number ensures correct fluorescence ratio convergence for each droplet size classes. From combined 3cLIF-PDA results, a mean local temperature T_m can be derived as following [16]:

$$T_m = \frac{\sum_{p=1}^{N_c} D_p^{2.8} N_p T_p}{\sum_{p=1}^{N} D_p^{2.8} N_p} \qquad (10)$$

where p is the droplet size class index, N_c the number of size classes, N_p the number of droplets per size class and T_p the temperature corresponding to the p^{th} class.

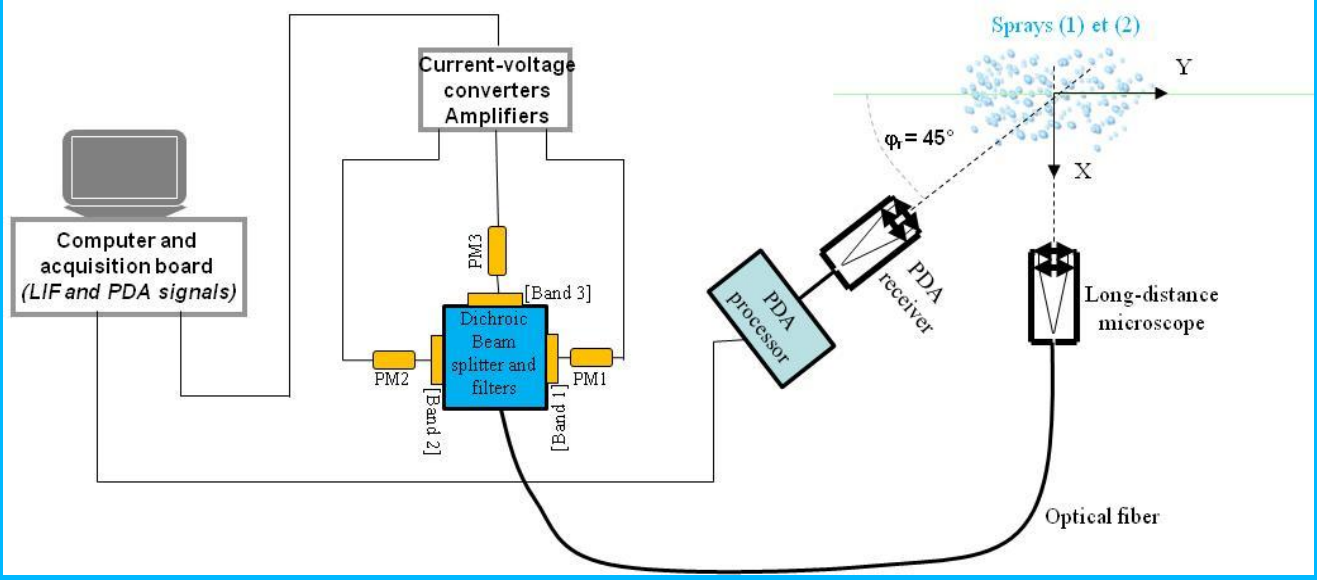

Figure 6: *Combined LIF/PDA experimental set-up (top view) and LIF optical set-up.*

4. Preliminary study

4.1 The sprays' characteristics

Fig. 7 gives typical droplet sizes distributions for spray (1) injected alone, for spray (2) injected alone and when both sprays were injected together. These distributions were measured at Z = 30 mm for $X = Y = 0$ at room temperature under isothermal conditions. The distributions were found to peak at about 15 µm for spray (1) and 30 µm for spray (2); the peak remains at 30 µm when the two sprays were operated together. In addition, measurements show that the droplet concentration of spray (1) was about a tenth of that of spray (2). This demonstrates clearly that under our operating conditions (*i.e.* Q_1= 20 ml/min with Q_2 = 40 ml/min or Q_2 = 60 ml/min), the second spray imposed the flow conditions.

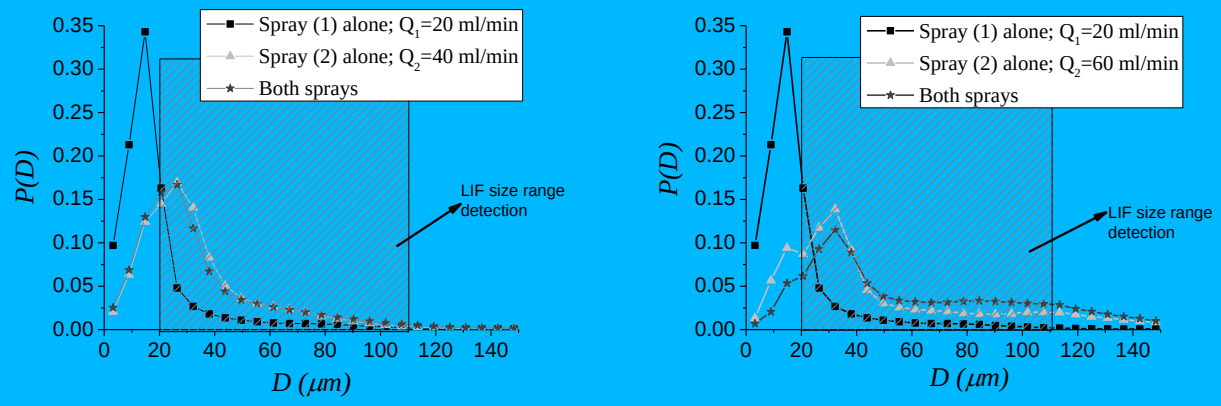

Figure 7: *Typical droplet size distributions measured at Z = 30 mm for spray (1) and spray (2), and when both are injected together. (a) Q_2 = 40 ml/min and (b) Q_2 = 60 ml/min. The detected droplet size range of LIF is also superimposed.*

4.2 Validation of the coupling device

In this section, preliminary results are presented in order to check the ability of the combined 3cLIF-PDA to investigate two interacting and non-isothermal sprays. In a first set of experiments,

each of the two sprays was injected alone, one having been pre-heated and the other one kept at ambient temperature. When the liquid was pre-heated, the injection temperature T_{inj} was fixed at 60 ± 2°C for the two sprays. All temperatures measured will be given in relation to this injection temperature. *Fig. 8* depicts the variation of the mean local temperature T_m along the Z-axis at $X = Y = 0$ and for both spray (1) and (2) injected separately and pre-heated or kept at ambient temperature (called hot or cold sprays respectively in the figure caption). When the spray was injected at ambient temperature, a small temperature decrease of about 5°C was observed which can be attributed to a moderate evaporation of the liquid. When the liquid was pre-heated, a strong decrease of the local spray temperature between the nozzle exit and the first measurement point at $Z = 30$ mm was found to occur. This cooling (around 17°C), was due to the heat transfer by forced convection with the gas phase. From $Z = 30$ mm up to $Z = 80$ mm the temperature decrease was found to continue moderately and also to be more important the higher the liquid flow rate. Cooling of about 3°C was observed for spray (1), 5°C for spray (2) with Q_1= 40 ml/min and 8°C for spray (2) with Q_2 = 60 ml/min. The mean droplet velocity, measured by the PDA and projected on the Z-axis, is shown in *Fig. 9.* It seemed that the vertical velocity of droplets was higher for spray (2), than for spray (1) regardless of the liquid flow rate. This means that the travel time of a droplet from the injection point to a current position in the spray was shorter for spray (2). The energy lost by the droplets through evaporation and forced convection was probably smaller in the case of spray (2) and this phenomenon was reinforced for the highest liquid flow rate. However, it should also be noted that this shorter heat transfer period was partially compensated by an increase in forced convection due to increased droplet velocity. In addition, the lower cooling for spray (2) could also be attributed to greater droplet concentration. Indeed, as this parameter increases with the flow rate, the vapor concentration due to droplet vaporization also increases. As measurements were taken on the sprays' median line where the droplet concentration was the highest, the presence of a noticeable amount of vapor could in fact have prevented evaporation and subsequent cooling.

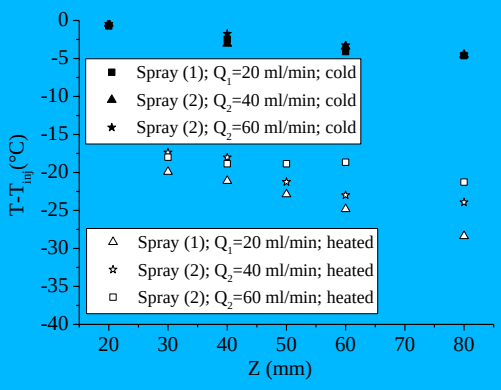

Figure 8: *Evolution of the mean droplet temperature along the Z axis for both sprays injected alone and injected at ambient temperature or preheated.*

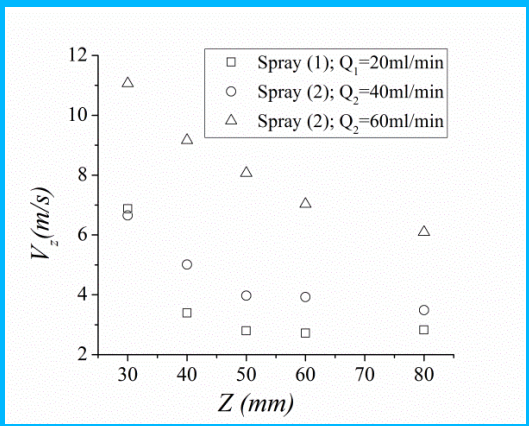

Figure 9: *Evolution of the vertical droplet velocity along the Z-axis for spray (1) and for spray (2) at Q_2 = 60 ml/min and Q_2 = 40 ml/min.*

Next, a second set of two experiments was run to check if the measurement technique and subsequent processing provided a good picture of the overall local enthalpy transported by the droplets. These were:

- First, sprays (1) and (2) were injected separately, spray (1) kept at ambient temperature, spray (2) having been pre-heated and temperature per droplet size class was measured using combined LIF and PDA for each of the spray.
  A local mean temperature T_{mh}, based on the local enthalpy transported by each of the sprays,

was calculated as follows:

$$T_{mh} = \frac{q_{m1}\sum_{p_1=1}^{N_{c1}} D_{p_1}^{2.8} N_{p_1} T_{p_1} + q_{m2}\sum_{p_2=1}^{N_{c2}} D_{p_2}^{2.8} N_{p_2} T_{p_2}}{q_{m1}\sum_{p_1=1}^{N_{c1}} D_{p_1}^{2.8} N_{p_1} + q_{m2}\sum_{p_2=1}^{N_{c2}} D_{p_2}^{2.8} N_{p_2}} \quad (11)$$

where p is the droplet size class index, N_c the number of size classes, N_p the number of droplets per size class, T_p the temperature corresponding to the p^{th} class and q_m the mass flux density (*i.e.* per unit time and per unit surface) measured by the PDA. Furthermore, indexes *1* and *2* denote the two sprays. In this equation, the first term and second term in the numerator represent the enthalpy of spray (1) and those of spray (2) respectively.

- Secondly, spray (1) and (2) were injected together in the same configuration as in the previous experiment. Consequently, the droplets that were detected and processed in a given location came either from spray (1) or (2). The local temperature was then determined using *eqn* (10).

The results obtained along the *Z*-axis are given in *Fig. 10*. Both evolutions were found to be very close together which proves the combined LIF-PDA technique has a good level of robustness. However, the temperature when the sprays were injected together was about 3°C higher than when they were injected separately. The interaction between the two sprays probably prevented heat transfers and the cooling down observed was smaller.

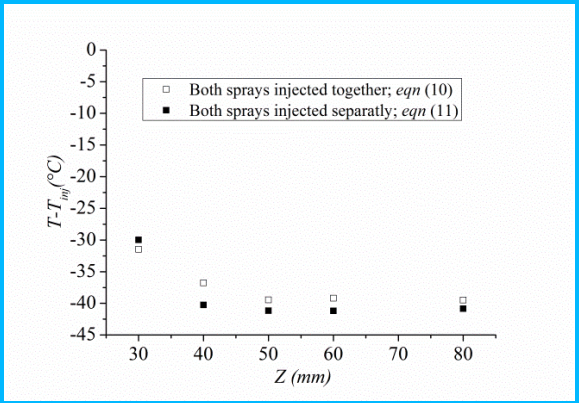

Figure 10: *Evolution of the mean droplet temperature along Z axis; comparison between eqn (10) and eqn (11).*

5. Investigation of the thermal mixing of two sprays

5.1 Spray (1) pre-heated

In this section, the results obtained according the following operating conditions are reported:
- Liquid of spray (1) was preheated with Q_1 = 20 ml/min and T_{inj} = 60 °C
- Liquid of spray (2) was kept at ambient temperature, with Q_2 = 40 ml/min and Q_2 = 60 ml/min

The evolution of the mean droplet temperature was first addressed before dealing with the evolution of the droplet temperature per size class. Finally, the heat transfer between the two sprays will be discussed.

Mean droplet temperature

Fig. 11 depicts the evolution of the mean local temperature (derived from *eqn* (10)) for spray (1) injected alone and for both sprays injected together with the two considered flow rates, Q_2 = 40 ml/min and Q_2 = 60 ml/min, along the *Z*-axis at $X = Y = 0$. In the case of spray (1) injected alone, a similar cooling of the droplets was observed as in *Fig. 8*. When the cold spray (2) was operated, an increase of the cooling on the spray along the Z-direction was clearly observed (*Fig. 11*). The

higher the flow rate of spray (2), the higher the rate of cooling was observed.

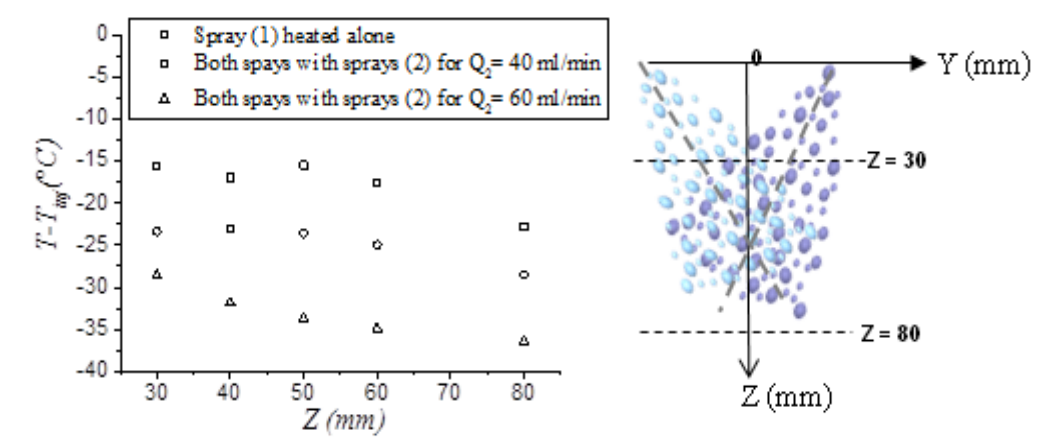

Figure 11: *Evolution of the mean droplet temperature along the Z axis for spray (1) heated and injected alone, and for spray (1) heated mixed with spray (2) for two flow rates at ambient temperature.*

Fig. 12 presents similar results obtained under similar conditions, but along the radial direction Y at $Z = 30$ mm. The position $Y = -17$ mm corresponds to the outer edge of the heated spray (1), $Y = -10$ mm is located on spray (1) centerline and $Y = 20$ mm corresponds to the outer edge of the cold spray (2). For spray (1) injected alone, a significant temperature increase was observed between the centerline ($Y = -10$ mm) and its edges with droplet temperature being about 5°C lower than in the center. No data is not available for $Y \geq 0$ since $Y = 0$ corresponds roughly to the inner edge of spray (1) and thus very little fluorescence signal could be collected. When both sprays were operated together, the influence of the cold droplets begins at $Y = -15$ mm and tends to lower the local mean droplet temperature.

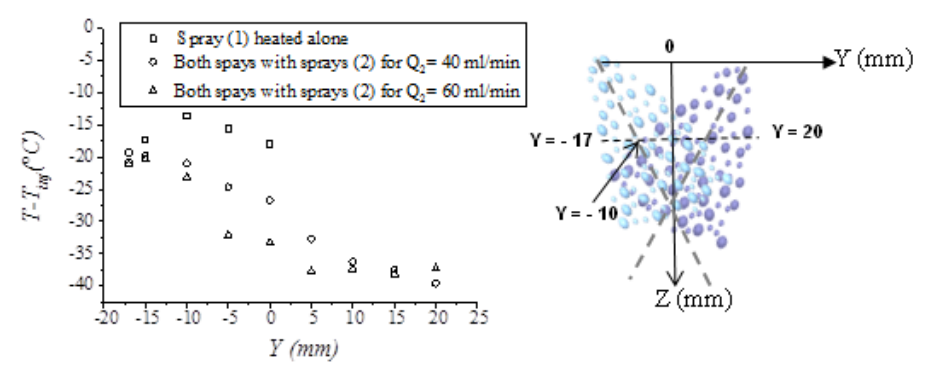

Figure 12: *Evolution of the mean droplet temperature along the Y axis at Z = 30 mm for spray (1) heated and injected alone, and for spray (1) heated mixed with spray (2) for two flow rates at ambient temperature.*

Droplet temperature per size class

The droplet temperature was also measured as a function of the droplet diameter by using combined 3cLIF-PDA, for different downstream positions. *Fig. 13a* gives an example of the results obtained at $Z = 30$ mm for three cases:

- spray (1) heated alone,
- both sprays operating with $Q_2 = 40$ ml/min and $Q_2 = 60$ ml/min.

As expected, the smallest droplets were associated with the lowest temperatures because they have the smallest thermal capacity. Droplets over 50 µm in diameter were found to have roughly the same temperature. We also noticed that, as with the mean temperature, the cooling of the droplets increased with the flow rate, regardless of the droplet size. *Fig. 13b-d* describes the evolution of the

droplet temperature along the Z-axis for the three cases and for three droplet size classes: D = 20 µm (b), D = 55 µm (c) and D = 100 µm (d). For D = 20 µm, the droplets seemed to have attained an equilibrium temperature for each of the investigated cases. For D = 55 µm, a temperature decrease was clearly observed for the three test cases and the cooling effect of spray (2) was both very visible and high in level. For D = 100 µm, the conclusion was similar but with a more pronounced temperature decrease.

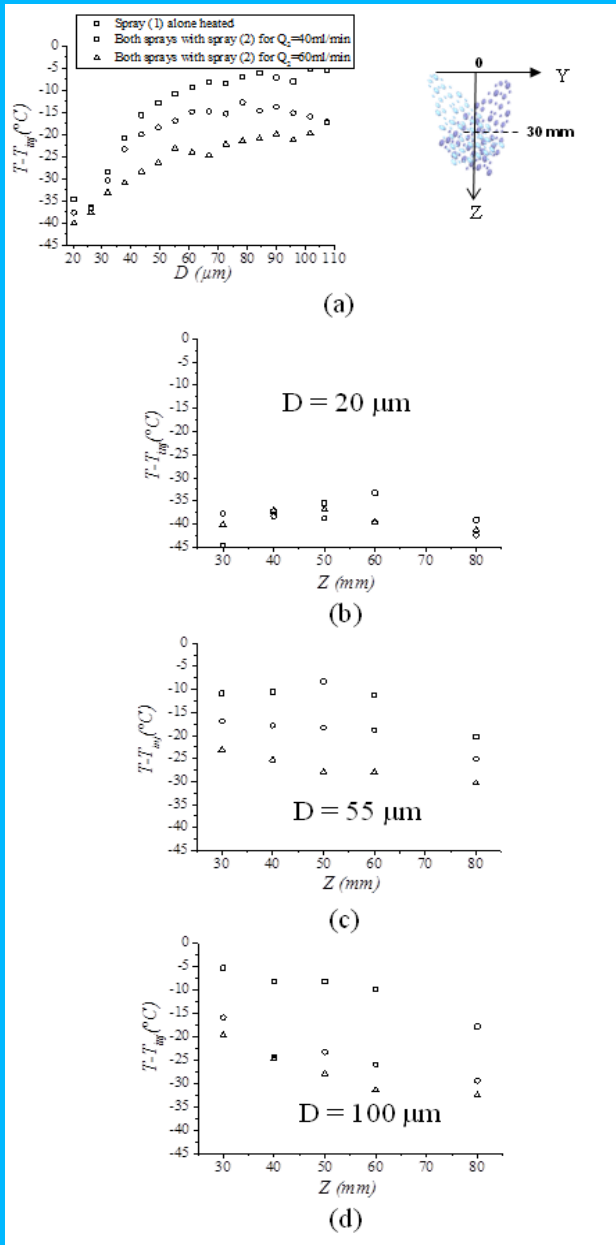

Figure 13: *(a): evolution of the droplet temperature as a function of the droplet diameter for spray (1) heated injected alone and for spray (1) heated mixed with spray (2) at two flow rates plotted at Z = 30 mm.(b)-(d): evolution of the droplet temperature along the Z-axis for three droplet size classes.*

Discussion about heat transfer between the two sprays

From previous results presented in *Fig. 11, 12 and 13* it is difficult to determine the nature of the mutual heat transfers between both sprays. Was heat transfer between the droplets due to

coalescence or was there an indirect influence due to vapor production or other kinds of aerodynamic interactions? Since the resulting local temperature measured by 3CLIF was calculated from droplets coming from both sprays, it is impossible to understand whether this mean temperature results from a superposition of hot and cold droplets or from real heat transfer between the two sprays. To find out more about this, one possibility is to measure the temperature of the droplets of spray (1) only. For that purpose, only the hot spray (1) was seeded with the fluorescent tracer whereas the cold spray (2) was only made up of pure water. This of course means that only the droplets coming directly from spray (1) may be detected. This set of experiments was carried out using only Q_2 = 40 ml/min for spray (2). Before performing these experiments, it was also necessary to check if the concentration of the dye remained constant. Indeed, if droplet coalescence occurred between a droplet seeded with the dye (*i.e.* coming from spray (1)) and a pure water droplet (*i.e.* coming from spray (2)), the dye would be diluted. As fluorescence intensity is proportional to dye concentration (*eqn* (1)), this means that during their transit time within the detection volume (*Fig.* 5), the droplets would induce a lower fluorescence intensity I_{fi}. To verify this hypothesis, the fluorescence intensity, collected on a spectral band, can be plotted as a function of the droplet diameter when spray (1) was injected alone and when both sprays were injected together. *Fig. 14* shows typical results obtained at Z = 30 mm and Y = – 10 mm. In this location, the droplet concentration was the highest when both sprays were operated together and therefore, the coalescence probability was at its maximum. It can be clearly observed that the fluorescence intensity remains almost identical proving that the fluorescent tracer concentration remains also almost constant. Therefore, the coalescence phenomena leading to thermal mixing probably remains marginal. Moreover, it is also interesting to compare the mean statistical distance l_m between two droplets with the mean droplet diameter D_{10}. The mean distance could be easily deduced from the droplet concentration C_d, obtained with the PDA, by:

$$l_m = \frac{1}{C_d^{1/3}} \qquad (12)$$

Fig. 15 shows the evolution of D_{10} and l_m along the Y-axis at Z = 30 mm, when both sprays were injected simultaneously. This clearly shows that the statistical mean distance between droplets is largely greater than the mean droplet diameter, which tends to minimize the probability of collisions.

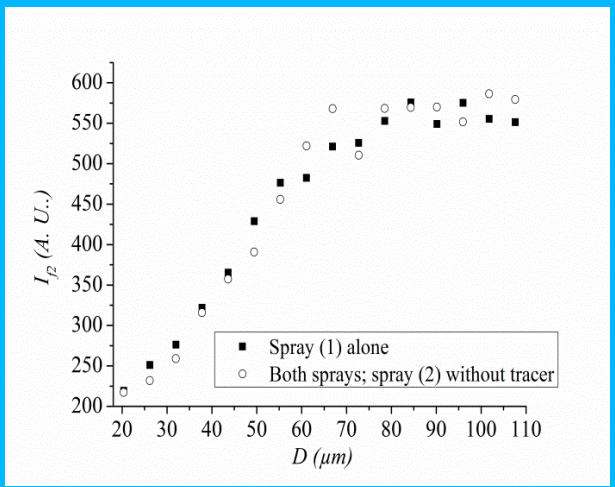

Figure 14: *Evolution of the fluorescence intensity on the second band of detection I_{f2} for spray (1) injected alone and for both sprays mixed when spray (2) is not seeded in fluorescence tracer.*

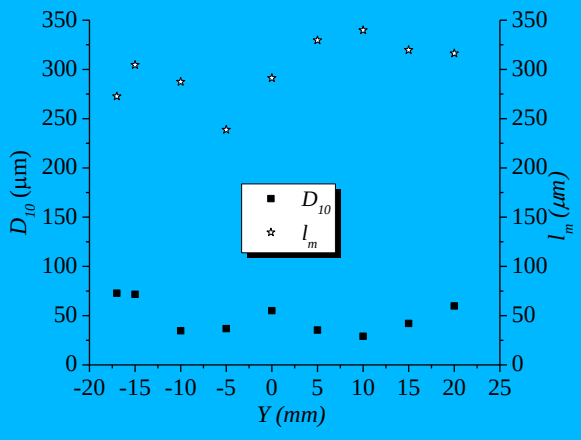

Figure 15: *Comparison between the mean distance between two droplets and the mean diameter along the Y axis at Z = 30 mm.*

Fig. 16 describes the evolution of the mean temperature along the *Z*-axis for five cases:

1) Spray (1) seeded by the fluorescent dye, heated and injected alone; symbols (■)
2) Spray (2) seeded by the fluorescent dye, injected alone at ambient temperature; symbols (☆)
3) Spray (1) heated, injected simultaneously with spray (2) and both sprays were seeded by the fluorescent dye; symbols (□)
4) Spray (1) heated, injected simultaneously with spray (2) but only spray (1) was seeded by the fluorescent dye; symbols (▲)
5) Spray (1) heated, injected simultaneously with spray (2) but only spray (2) was seeded in fluorescent dye; symbols (○)

The analysis of these measurements leads to three statements:

- The temperature evolutions along *Z* were found to be almost similar in cases 1 and 4, although the temperature was a few degrees lower when the two sprays were mixed together. This could reveal a moderate degree of interaction between the droplets oncoming from the heated spray with those from the cold spray. However, we should remain cautious about drawing a definite conclusion on this point because of uncertainty about the temperature measured by 3cLIC [18].
- This statement is confirmed by the comparison of cases 2 and 5: the evolution of the temperature of the mixed sprays was nearly similar to this of spray (2). It should also be noted that the temperature of the mixed sprays was a few degrees higher than for spray (2) alone, which reveals also a small degree of interaction between both sprays.
- Case 3 is intermediate: temperature evolution showed that the mean spray local temperature was calculated with droplets oncoming from the heated and cold spray.

The evolution of the droplet temperature as a function of the diameter class is presented in *Fig. 17* for the previous cases 1, 2, 4 and 5, at $Z = 30$ mm. The results confirm the statements obtained for the mean temperature. Again the cold spray seems to only have a marginal influence on the heated spray regardless of droplet diameter. The measurements of the temperature per droplet size class are less accurate than the measurement of mean temperature which means it was not possible to observe the moderate interaction between the hot and cold droplets mentioned above.

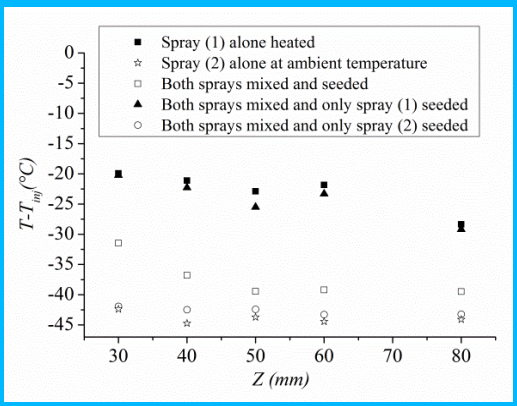

Figure 16: *Evolution of the mean droplet temperature along the Z axis for spray (1) alone (heated or at ambient temperature) and for both sprays mixed when both or only one are seeded in fluorescence tracer.*

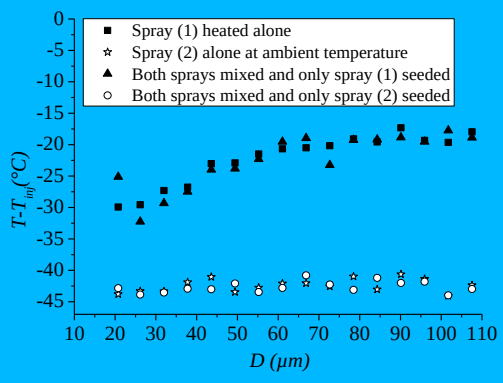

Figure 17: *Evolution of the droplet temperature as a function of the droplet diameter at Z = 30 mm for both sprays injected alone or mixed and when both sprays are seeded or only one.*

5.2 Spray (2) pre-heated

This section presents the measurements for the case for which the liquid of spray (2) was pre-heated

at T_{inj} = 60 °C whereas the liquid of spray (1) was kept at ambient temperature. These experiments were performed with only Q_2 = 40 ml/min for spray (2). *Fig. 18* depicts the evolution of the liquid temperature along the *Z*-axis for four cases:

1) Spray (2) heated and injected alone; symbols (■)
2) Spray (2) heated and injected simultaneously with spray (1) and both sprays were seeded with the fluorescent tracer; symbols (□)
3) Spray (2) heated and injected simultaneously with spray (1) but only spray (1) was seeded with the fluorescent tracer; symbols (▲)
4) Spray (1) seeded with the fluorescent tracer and injected alone at ambient temperature; symbols (☆)

When spray (2) was injected alone, the cooling mentioned earlier was observed (*Fig. 8)*. The heating observed in case (2), when both sprays were injected together, was found to be surprising. The local spray temperature evidently appears lower than in the case of spray (2) injected alone at Z=30 mm, due to the contribution of cold droplets oncoming from spray (1). However, the temperature measured when the two sprays were interacting, began to increase beyond Z = 40 mm and reached the temperature of spray (2), injected alone, at Z = 80 mm. The most probable explanation for this phenomenon is that the droplets of spray (1) moved in the hot vapor produced by spray (2). Clearly it is logical for this contribution to be noticeable given that the liquid flow rate of spray (2) is twice the flow rate of spray (1). The temperature of the two sprays tended to be the same equilibrium value in the vicinity of Z = 80 mm. This phenomenon was not noticed when spray (1) was heated due to its lower liquid flow rate. The heating of spray (1) in the presence of spray (2) is confirmed by our analysis of results for case 3 - where only the droplets of spray (1) are visualized. Case 4 confirms that spray (1) injected alone at the ambient temperature remained at almost constant temperatures although a moderate cooling can be observed due to evaporation.

Fig. 19 presents the droplet temperature evolution per size class, for both sprays mixed together, when only spray (1) was seeded with the fluorescent tracer, at Z = 30 mm and Z = 80 mm. The heating of the droplet of spray (1) was clearly visible and seemed to affect droplets of under 70 µm in diameter more than bigger droplets although interpretation of these results is difficult given the limited accuracy of the measurements.

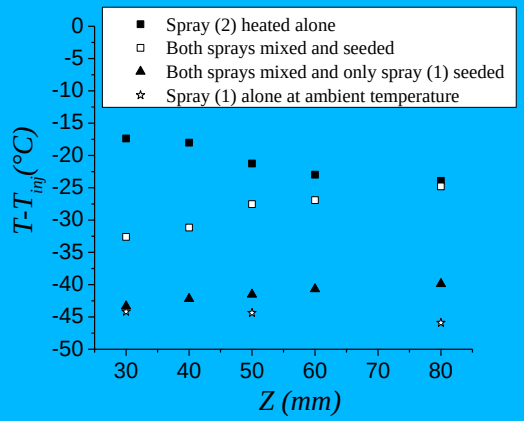

Figure 18: *Evolution of the mean droplet temperature along the Z axis for spray (2) alone (heated or at ambient temperature) and for both sprays mixed when both or only one are seeded in fluorescence tracer.*

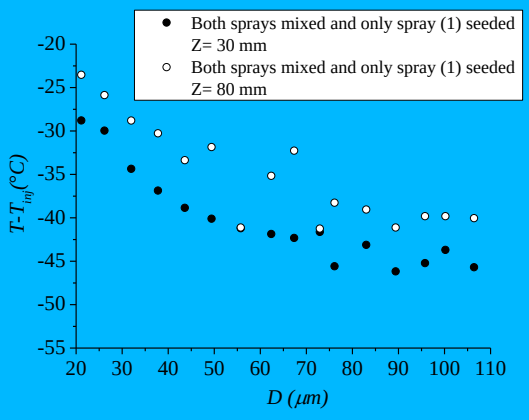

Figure 19: *Evolution of the droplet temperature as a function of the droplet diameter at Z = 30 mm and Z = 80 mm for both sprays injected when only spray (1) is seeded.*

6. Conclusions

A combination of three-color laser induced fluorescence (3cLIF) thermometry and Phase Doppler

measurements was used to study the mixing of two polydisperse sprays with various injection conditions. This technique clearly demonstrated its ability to determine the nature of the thermal mixing of two sprays and the related heat transfers that may occur. In the cases investigated in the present study, the degree of mixing due to the coalescence of droplets was probably marginal. However, the effect of the temperature on the local mean liquid temperature was clearly highlighted. Indirect heat transfer from one spray to the other was also established due to the production of a significant amount of hot vapor by the heated spray with a large liquid flow rate.
The work presented in this paper was our first attempt to perform measurements in this kind of mixing situation and will be reproduced using denser sprays where droplet coalescence should have a significant influence.
.

References

[1] Sazhin, (2006), Advanced models for fuel droplets heating and evaporation, *Pro Energy Comb Sci*, 32: 162-214.
[2] Maqua et al., (2008), Monodisperse droplet heating and evaporation: Experimental study and modeling, *Int J Heat Mass Transfer*, 51: 3932-3945.
[3] Depredurand V et al., (2011), Combined PDA and LIF applied to size-temperature correlations measurements in heated spray, *Exp Fluids*, 50: 561-571.
[4] Castanet et al., (2009), Dynamics and temperature of droplets impacting onto a heated wall. *Int J Heat Mass Transfer*, 52: 670-679.
[5] Bernardin et al., (1997), Mapping of impact and heat transfer regimes of water drops impinging on a polished surface, *Int J Heat Mass Transfer*, 40**:** 247–267.
[6] Roisman and Tropea, (2001), Flux measurements in sprays using Phase Doppler techniques, *Atom Sprays*, 11: 673-705.
[7] Van Beek et al., (2003), Global rainbow thermometry assessed by airy and Lonrenz-Mie theories and compared with phase Doppler anemometry, *App Opt*, 42: 4016-4022.
[8] Vetrano et al., (2006), Characterization of a non-thermal water spray by global rainbow thermometry, *Exp Fluids*, 50: 15-22.
[9] Sawitree et al., (2010), Processing of individual rainbow signals to study droplets evaporation, *Exp Fluids*, 48: 111-119.
[10] Sawitree et al., (2009), Experimental analysis of global rainbow technique: sensitivity of temperature and size distribution measurements to non-spherical droplets, *Exp Fluids*, 47: 839-848.
[11] Murray et al., (1985), Fluorescence methods for determination of temperature in fuel spray, *App Opt*, 24: 2783-2787.
[12] Gossage et al., (1987), Fluorescence thermometers using intermolecular exciplex, *Appl Opt*, 26: 2256-2259
[13] Sakakibara et al., (1999), Whole Field Measurement of Temperature in Water Using Two-Color Laser Induced Fluorescence, *Exp Fluids*, 26: 7-15.
[14] Kim et al., (2003), Examination of a Ratiometric Laser Induced Fluorescence Thermometry for Microscale Spatial Measurement Resolution, *Int J Heat Mass Transfer*, 46: 3967-3974.
[15] Lavieille et al., (2001), Evaporating and combusting droplet temperature measurements using two-color laser-induced fluorescence, *Exp Fluids*, 31: 45-55.
[16] Castanet et al., (2003), Measurement of the temperature distribution within monodisperse combusting droplets in linear streams using two-color laser-induced fluorescence, *Exp Fluids*, 35: 563-571.
[17] Labergue et al., (2010), New insight into two-color LIF thermometry applied to temperature measurements of droplets, *Exp Fluids*, 49: 547-556.
[18] Labergue et al., (2012), Study of the droplet size effect coupled with the laser light scattering in sprays for two-color LIF thermometry, *Exp Fluids*, 52: 1121-1132.
[19] Depredurand et al., (2008), A temperature-sensitive tracer suitable for two-color laser-induced fluorescence thermometry applied to evaporating fuel droplets, *Meas Sci Technol*, 19: 1-12.